IEEE Access
Multidisciplinary | Rapid Review | Open Access Journal

Received December 29, 2017, accepted January 27, 2018, date of publication February 2, 2018, date of current version March 12, 2018.

Digital Object Identifier 10.1109/ACCESS.2018.2801351

Precision Cascade Force Control of Multi-DOF Hydraulic Leg Exoskeleton

SHAN CHEN[1], ZHENG CHEN[2,3], (Member, IEEE), AND BIN YAO[2,4], (Senior Member, IEEE)

[1]School of Mechanical Engineering, Hefei University of Technology, Hefei 230009, China
[2]State Key Laboratory of Fluid Power and Mechatronic Systems, Zhejiang University, Hangzhou 310027, China
[3]Ocean College, Zhejiang University, Hangzhou 310027, China
[4]School of Mechanical Engineering, Purdue University, West Lafayette, IN 47907, USA

Corresponding author: Zheng Chen (zheng_chen@zju.edu.cn)

This work was supported in part by the National Natural Science Foundation of China under Grant U1609211, Grant 61603332, and Grant 61633019, and in part by the Science Fund for Creative Research Groups of National Natural Science Foundation of China under Grant 51521064.

ABSTRACT Hydraulic exoskeleton is a kind of the human robot interaction system, which can augment the human performance in the application of heavy load carrying. Due to the existence of complicated multi-joint nonlinear dynamics and various uncertainties, traditional robust control of these systems is hard to be realized in most of the practical research. In this paper, an adaptive robust cascade force controller is proposed for 3-DOF hydraulic leg exoskeleton to achieve accurate tracking of human motion. Specifically, the control strategy includes two levels. The desired joint positions, which can be assumed as the human motion intent as well, are generated in the high-level by attenuating the integral of human–machine interaction force. And in the low-level, an observer-based MIMO motion controller is developed for 3-DOF dynamics to track the generated human motion intent accurately. Adaptive robust control algorithms are developed in both control levels to address the strongly coupled high-order dynamics under parametric uncertainties and uncertain disturbances. Comparative simulations show that the human–machine interaction force can be attenuated exactly and robust performance to various uncertainties can be guaranteed, validating the effectiveness of the proposed scheme.

INDEX TERMS Adaptive robust control, cascade control, hydraulic exoskeleton, multi-joint coupling, observer design.

I. INTRODUCTION

Lower limb exoskeletons for human performance augmentation are wearable robots which guarantee the wearer's endurance and agility when walking with heavy loads [1]. As a typical human machine interaction system, robot power and human intelligence are integrated perfectly in the system leading to a good performance in unstructured environment. Specifically, the heavy load mounted on the exoskeleton is supported by the exoskeleton actuators while the healthy operator gives the motion commands that the exoskeleton needs to follow. Due to the small size-to-power ratio and the ability to provide high force and torque, hydraulic actuators are often selected in these exoskeleton systems. When the exoskeleton can track the human motion accurately, the heavy load is transferred to the ground through the exoskeleton and the human almost can not feel the existence of the load, and thus can complete various actions flexibly. Therefore, the high performance human machine synchronization control algorithm design becomes the key technology in the development of lower limb exoskeleton for human performance augmentation.

Various control schemes have been designed to improve the performance of exoskeletons, which can be divided into two types. In the first type, the human-machine interaction force is not measured directly. Typical examples include the virtual joint force control [1], sensitivity amplification control (SAC) [2], and fictitious gain method [3]. Since it is impossible to obtain a precise inverse dynamics, robust performance of these control methods usually cannot be guaranteed. Also, because of the large compressibility of hydraulic oil, the output force of the hydraulic actuator is hard to be tracked. Thus the performance of the above interaction force controllers in which the control input should be the joint torque are often quite limited in hydraulic exoskeleton systems. In another category, such as admittance control [4], [5] and human machine cooperation controller design [6], a direct

measurement of human-machine interaction force is done. In these approaches, the two-level cascade control structure is adopted. Often the human motion intent is inferred in the high level controller while the motion tracking is done in the low level. However, because of using human data to infer the human motion intent, the method in [4] and [5] can not be easily generalized to various wearers which limits the effectiveness in practical implementation. In [6], the desired position is generated by a model-free PID force controller. However, the robust performance of the controller is poor due to the neglect of the model uncertainties in the algorithm design. Also, it is not clear how to tune the gains of the PID controller. Other exoskeleton force control methods such as [7]–[9] are developed for motor driven systems. It is known that the presence of complicated nonlinear dynamics and various types of model uncertainties in the hydraulic actuators makes it more challenging to control hydraulically actuated exoskeleton.

To solve this problem, an adaptive robust cascade force controller is proposed in [10] for 1-DOF hydraulic exoskeleton system. Parameter uncertainties and uncertain nonlinearities are considered in the modeling and be addressed effectively through the adaptive robust control (ARC) algorithms. In this paper, the problem is extended to more practical and typical 3-DOF leg exoskeleton, which leads to more challenging issues. The system in study has various types of model uncertainties, including the appearance of unknown parameters in the inertia matrix which makes the joint acceleration can not be linearly parameterized. In the controller design, the integral of human-machine interaction force are minimized to generate the desired positions in the high level (which can also be seen as the human motion intent). In the low level, different from the 1-DOF controller design, an additional observer is first synthesized to estimate the joint acceleration which is needed in the following motion tracking controller design. Then, a MIMO motion tracking controller using backstepping technique is designed. ARC algorithms are applied in both control levels to effectively handle all the uncertainties for a guaranteed robust performance.

II. DYNAMICAL MODELS

The 3-DOF hydraulically actuated support leg exoskeleton system as shown in Fig. 1 includes three parts: the hydraulic actuators, the 3-DOF mechanic system(including the load), and the human-machine interface resulting from the physical contact between the exoskeleton and the human. The human machine contact point is on the back. With only considering the compliant properties in the interface and also neglecting the valve dynamics, the overall system dynamics can be described by Eq.(1) [11]

$$\begin{aligned} F_{hm} &= K(x_h - x_e) + \tilde{D}_1 \\ q &= invkine(x_e) \\ \tau_{act} + J^T(q)F_{hm} &= M_{sp3}(q)\ddot{q} + C_{sp3}(q,\dot{q})\dot{q} \\ &\quad + G_{sp3}(q) + B\dot{q} + \tilde{D}_2 \end{aligned}$$

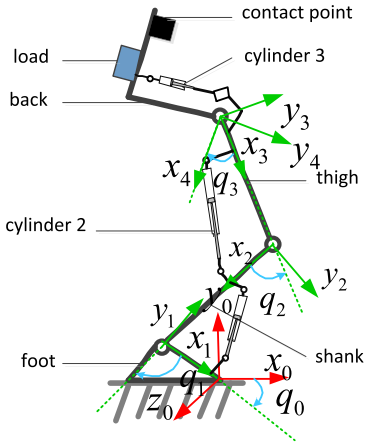

FIGURE 1. 3-DOF hydraulic support leg exoskeleton system.

$$\begin{aligned} \tau_{act} &= [\,\tau_1 \quad \tau_2 \quad \tau_3\,]^T, \\ \tau_i &= (P_{1i}A_{1i} - P_{2i}A_{2i})\frac{\partial x_{Li}}{\partial q_i} \\ \frac{V_{1i}}{\beta_e}\dot{P}_{1i} &= -A_{1i}\frac{\partial x_{Li}}{\partial q_i}\dot{q}_i + Q_{1i} + \tilde{D}_{31i} \\ \frac{V_{2i}}{\beta_e}\dot{P}_{2i} &= A_{2i}\frac{\partial x_{Li}}{\partial q_i}\dot{q}_i - Q_{2i} + \tilde{D}_{32i} \\ Q_{1i} &= k_{q1i}x_{vi}\sqrt{|\Delta P_{1i}|}, \quad Q_{2i} = k_{q2i}x_{vi}\sqrt{|\Delta P_{2i}|} \\ \Delta P_{1i} &= \begin{cases} P_s - P_{1i} & if\ x_{vi} \geq 0 \\ P_{1i} - P_r & if\ x_{vi} < 0 \end{cases} \\ \Delta P_{2i} &= \begin{cases} P_{2i} - P_r & if\ x_{vi} \geq 0 \\ P_s - P_{2i} & if\ x_{vi} < 0 \end{cases} \\ x_{vi} &= u_i, \quad i = 1, 2, 3 \end{aligned} \tag{1}$$

where $F_{hm} = \left[F_x\ F_y\ \tau_z\right]^T$ is the human-machine interaction force at the contact point. $K = diag\{K_x, K_y, K_z\}$ represents the stiffness of the human-machine interface. $x_h = \left[x_{hx}\ x_{hy}\ \theta_{hz}\right]^T$ and $x_e = \left[x_{ex}\ x_{ey}\ \theta_{ez}\right]^T$ represent the human position and exoskeleton position at the contact point, respectively. $q = \left[q_1\ q_2\ q_3\right]^T$ represents the joint position and can be related to x_e by the inverse kinematics, which denotes as $q = invkine(x_e)$. τ_{act} is the joint torque from the actuators. $J(q) = \frac{\partial x_e}{\partial q}$ is the Jacobian matrix. $M_{sp3}(q)$, $C_{sp3}(q,\dot{q})\dot{q}$, $G_{sp3}(q)$ represent the inertial matrix, centrifugal/Coriolis force and gravity force, respectively. $B = diag\{B_1, B_2, B_3\}$ is the damping ratio. x_{Li} is the displacement of the cylinder i and $\partial x_{Li}/\partial q_i$ represents the first-order partial derivative of x_{Li} with respect to q_i. P_{1i}, P_{2i}, A_{1i} and A_{2i} represent the absolute pressures and the acting areas of the two chambers in cylinder i, respectively. $V_{1i} = V_{h1i} + A_{1i} \cdot x_{Li}$ and $V_{2i} = V_{h2i} - A_{2i} \cdot x_{Li}$ are total volumes of two chambers in cylinder i. V_{h1i}, V_{h2i} are two chamber volumes when $q_i = 0$. β_e represents the effective bulk modulus. Q_{1i}, Q_{2i} are the supply and return flow of cylinder i, respectively. k_{q1i} and k_{q2i} are the flow gain coefficients for the two loops of cylinder i, respectively. x_{vi} is the spool displacement of valve i. P_s is the supply pressure and P_r is the pressure in the tank. $\tilde{D}_1$, $\tilde{D}_2$, $\tilde{D}_{31i}$, and $\tilde{D}_{32i}$ represent the lumped modeling errors and uncertain disturbances in each dynamic model.

The first equation of (1) is algebraic in nature. As shown in [12]–[14], integral force feedback control is more suitable for algebraic type of model. Thus the integral of interaction force $\int_0^t F_{hm}d\tau$ is adopted in the controller design. Finally, a first order dynamics from x_e to $\int_0^t F_{hm}d\tau$ is obtained as

$$\frac{d}{dt}\int_0^t F_{hm}d\tau = K(x_h - x_e) + \tilde{D}_1 \tag{2}$$

The third equation of (1) has the following properties that will facilitate the controller design.

Property 1: For the finite workspace Ω_q in which all kinematic transformation are well defined, $M_{Sp3}(q)$ is an s.p.d. matrix with $k_r' I_3 \le M_{Sp3}(q) \le k_r'' I_3$, where k_r', k_r'' are some positive constants and I_3 represents an 3×3 identity matrix.

Property 2: The matrix $\dot{M}_{Sp3}(q) - 2C_{Sp3}(q,\dot{q})$ is a skew-symmetric matrix.

Property 3: $M_{Sp3}(q)$, $C_{Sp3}(q,\dot{q})$, $G_{Sp3}(q)$ can be linearly parameterized in terms of β, i.e.,

$$\begin{aligned} M_{Sp3}(q)\ddot{q}_r + C_{Sp3}(q,\dot{q})\dot{q}_r + G_{Sp3}(q) \\ = f_0(q,\dot{q},\dot{q}_r,\ddot{q}_r) + Y(q,\dot{q},\dot{q}_r,\ddot{q}_r)\beta \end{aligned} \tag{3}$$

where $\dot{q}_r, \ddot{q}_r$ are any reference vector. β is the system parameters related to the leg exoskeleton.

III. CONTROLLER DESIGN

A. DESIGN MODEL AND CONTROL OBJECTIVE

Define the following lumped disturbances and parameter vectors:

$$\begin{aligned}
\tilde{\Delta}_1 &= x_h + K^{-1}\tilde{D}_1,\ \tilde{\Delta}_3 = -\tilde{D}_2 \\
\tilde{\Delta}_4 &= [\tilde{D}_{311}\frac{\beta_e A_{11}}{V_{11}} - \tilde{D}_{321}\frac{\beta_e A_{21}}{V_{21}}, \tilde{D}_{312}\frac{\beta_e A_{12}}{V_{12}} \\
&\quad - \tilde{D}_{322}\frac{\beta_e A_{22}}{V_{22}}, \tilde{D}_{313}\frac{\beta_e A_{13}}{V_{13}} - \tilde{D}_{323}\frac{\beta_e A_{23}}{V_{23}}]^T \\
\tilde{\Delta}_i &= \Delta_{in} + \Delta_i, \quad i = 1,3,4
\end{aligned} \tag{4a}$$

$$\begin{aligned}
K_\theta &= \begin{bmatrix} 1/K_x & 1/K_y & 1/K_z \end{bmatrix}^T \\
\Delta_{1n} &= \begin{bmatrix} \Delta_{1nx} & \Delta_{1ny} & \Delta_{1nz} \end{bmatrix}^T \\
B_\theta &= \begin{bmatrix} B_1 & B_2 & B_3 \end{bmatrix}^T \\
\Delta_{3n} &= \begin{bmatrix} \Delta_{3n1} & \Delta_{3n2} & \Delta_{3n3} \end{bmatrix}^T \\
\Delta_{4n} &= \begin{bmatrix} \Delta_{4n1} & \Delta_{4n2} & \Delta_{4n3} \end{bmatrix}^T \\
\theta_F &= \begin{bmatrix} K_\theta^T & \Delta_{1n}^T \end{bmatrix}^T \\
\theta_q &= \begin{bmatrix} \beta^T & B_\theta^T & \Delta_{3n}{}^T & \beta_e & \Delta_{4n}{}^T \end{bmatrix}^T \\
\theta &= \begin{bmatrix} \theta_F^T & \theta_q^T \end{bmatrix}^T
\end{aligned} \tag{4b}$$

where Δ_{in} and Δ_i represent the constant and time-varying part of $\tilde{\Delta}_i$, respectively. Assume that $\theta \in \Omega_\theta \triangleq \{\theta : \theta_{\min} \le \theta \le \theta_{\max}\}$ and $|\tilde{\Delta}| \le \delta_d(t,x)$ where $\theta_{\min} = [\theta_{1\min}, \cdots, \theta_{17\min}]^T$, $\theta_{\max} = [\theta_{1\max}, \cdots, \theta_{17\max}]^T$, and $\delta_d(t,x)$ is known.

Define the following state variables:

$$\begin{aligned}
x_1 &= \begin{bmatrix} \int_0^t F_x d\tau & \int_0^t F_y d\tau & \int_0^t \tau_z d\tau \end{bmatrix}^T \\
x_2 &= q, \quad x_3 = \dot{q} \\
x_4 &= P_1 = \begin{bmatrix} P_{11} & P_{12} & P_{13} \end{bmatrix}^T \\
x_5 &= P_2 = \begin{bmatrix} P_{21} & P_{22} & P_{23} \end{bmatrix}^T \\
x &= \begin{bmatrix} x_1^T & x_2{}^T & x_3{}^T & x_4{}^T & x_5{}^T \end{bmatrix}^T
\end{aligned} \tag{5}$$

and the state-space form of system dynamics (1) can be expressed as:

$$\begin{aligned}
\dot{x}_1 &= -Kx_e + K\Delta_{1n} + K\Delta_1 \\
x_2 &= invkine(x_e) \\
\dot{x}_2 &= x_3 \\
\dot{x}_3 &= M_{Sp3}^{-1}(x_2)[hP_L + J^T F_{hm} - C_{Sp3}(x_2,x_3)x_3 \\
&\quad - G_{Sp3}(x_2) - Bx_3 + \Delta_{3n} + \Delta_3] \\
\dot{P}_L &= Q_L\beta_e - q_v x_3 \beta_e + \Delta_{4n} + \Delta_4 \\
Q_L &= K_q u
\end{aligned} \tag{6}$$

where *invkine* denotes the inverse kinematics.

$$\begin{aligned}
h &= diag\{\frac{\partial x_{L1}}{\partial q_1}, \frac{\partial x_{L2}}{\partial q_2}, \frac{\partial x_{L3}}{\partial q_3}\}. \\
A_1 &= diag\{A_{11}, A_{12}, A_{13}\}. \\
A_2 &= diag\{A_{21}, A_{22}, A_{23}\}. \\
P_L &= A_1 x_4 - A_2 x_5. \\
Q_L &= \Big[\frac{Q_{11}A_{11}}{V_{11}} + \frac{Q_{21}A_{21}}{V_{21}}, \frac{Q_{12}A_{12}}{V_{12}} \\
&\quad + \frac{Q_{22}A_{22}}{V_{22}}, \frac{Q_{13}A_{13}}{V_{13}} + \frac{Q_{23}A_{23}}{V_{23}}\Big]^T. \\
q_v &= diag\{(\frac{A_{11}^2}{V_{11}} + \frac{A_{21}^2}{V_{21}})\frac{\partial x_{L1}}{\partial q_1}, (\frac{A_{12}^2}{V_{12}} + \frac{A_{22}^2}{V_{22}})\frac{\partial x_{L2}}{\partial q_2}, \\
&\quad \times(\frac{A_{13}^2}{V_{13}} + \frac{A_{23}^2}{V_{23}})\frac{\partial x_{L3}}{\partial q_3}\}. \\
K_q &= diag\{k_{q11}\frac{A_{11}}{V_{11}}\sqrt{|\Delta P_{11}|} + k_{q21}\frac{A_{21}}{V_{21}}\sqrt{|\Delta P_{21}|}, \\
&\quad \times k_{q12}\frac{A_{12}}{V_{12}}\sqrt{|\Delta P_{12}|} + k_{q22}\frac{A_{22}}{V_{22}}\sqrt{|\Delta P_{22}|}, \\
&\quad \times k_{q13}\frac{A_{11}}{V_{13}}\sqrt{|\Delta P_{13}|} + k_{q23}\frac{A_{23}}{V_{23}}\sqrt{|\Delta P_{23}|}\}
\end{aligned}$$

Under the situation that the wearer is capable of executing the necessary motions for achieving locomotion, the exoskeleton is only asked to follow the human motion quickly and accurately. Thus, the control objective is to design a control input $u = \begin{bmatrix} u_1 & u_2 & u_3 \end{bmatrix}^T$ based on Eq.(6) so that the human machine interaction force F_{hm} can be minimized and accurate motion tracking of exoskeleton output x_e to human motion x_h can be achieved.

B. OVERALL CONTROL STRUCTURE

Fig. 2 shows the block diagram of the adopted cascade force controller. As for the control of hydraulic systems with various uncertainties, much work has been done [15]–[18].

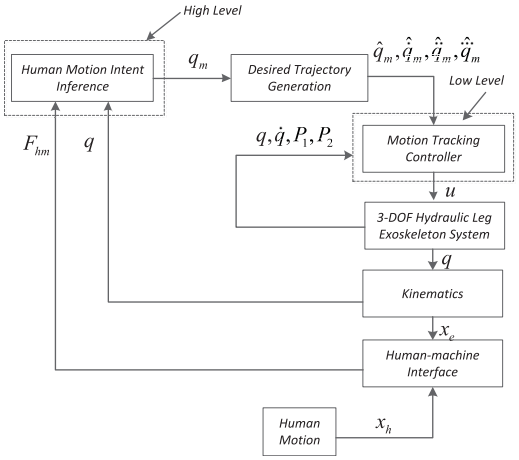

FIGURE 2. Overall control structure.

The ARC [19], [20] is an effective control algorithm to address both parametric uncertainties and uncertain nonlinearities with a number of successful applications [21]–[26]. Thus, it will be applied in our proposed force controller design. Actually, the control architecture of the proposed method is similar with admittance control. They both adopt the cascade architecture in which the outer loop force controller is in series to the inner loop position controller. However, the detailed control algorithms are quite different.

C. HIGH-LEVEL HUMAN MOTION INTENT INFERENCE

With the position of exoskeleton x_e treated as the virtual control input, the control objective of high level controller is to generate a virtual control law x_m for x_e so that the integral of force tracking error $z_1 = x_1 - x_{1d}$ can converge to zero or to be bounded. x_{1d} is the desired trajectory to be tracked by x_1. Depending on the actual application requirements, the desired human machine interaction force can be selected as zero or as a scaled-down version of the load force. Define $K_f = K^{-1}$. The following can be obtained considering K_f is linear w.r.t. θ_F

$$K_f \dot{x}_{1d} - \Delta_{1n} = f_{\theta_F}(\dot{x}_{1d}) + Y_{\theta_F}(\dot{x}_{1d})\theta_F \tag{7}$$

where $f_{\theta_F}, Y_{\theta_F}$ are known. From the first equation of (6), the error dynamics becomes

$$K_f \dot{z}_1 = -x_e + \Delta_{1n} + \Delta_1 - K_f \dot{x}_{1d} \tag{8}$$

The following ARC control strategy is designed:

$$\begin{aligned} x_m &= x_{ma} + x_{ms} \\ x_{ma} &= -\hat{K}_f \dot{x}_{1d} + \hat{\Delta}_{1n} = -f_{\theta_F}(\dot{x}_{1d}) - Y_{\theta_F}(\dot{x}_{1d})\hat{\theta}_F \\ x_{ms} &= K_1 z_1 + x_{msn} \\ \dot{\hat{\theta}}_F &= Proj(-\Gamma_1 Y_{\theta_F}^T z_1) \\ Proj_i(\bullet_i) &= \begin{cases} 0 & \text{if } \hat{\theta}_{Fi} = \theta_{F\max i} \text{ and } \bullet_i > 0 \\ 0 & \text{if } \hat{\theta}_{Fi} = \theta_{F\min i} \text{ and } \bullet_i < 0 \\ \bullet_i & \text{otherwise} \end{cases} \end{aligned} \tag{9}$$

where x_{ma} and x_{ms} represent the model compensation and robust feedback term, respectively. K_1 and Γ_1 represent the positive definite matrix for linear feedback and adaptation rate, respectively. x_{msn} is a robust control function having the following two properties:

$$\begin{aligned} z_1^T \left(\Delta_1 + \frac{1}{2}\dot{K}_f z_1 + Y_{\theta_F}\tilde{\theta}_F - x_{msn} \right) &\le \varepsilon_1 \\ -z_1^T x_{msn} &\le 0 \end{aligned} \tag{10}$$

where $\varepsilon_1 > 0$ is a design parameter. $\tilde{\theta}_F = \hat{\theta}_F - \theta_F$ is the parameter estimation error. Define $z_{2h} = x_e - x_m$, the first error subsystem becomes

$$K_f \dot{z}_1 = -K_1 z_1 - z_{2h} + \Delta_1 + Y_{\theta_F}\tilde{\theta}_F - x_{msn} \tag{11}$$

It is seen that when the exoskeleton tracks the desired position x_m, the interaction force can be minimized. Thus the virtual control law x_m can be regarded as the human motion intent. Finally the desired joint position q_m can be solved by

$$q_m = invkine(x_m) \tag{12}$$

D. DESIRED TRAJECTORY GENERATION

The same as [10], the desired motion trajectories of the exoskeleton joints are obtained through the following output differential observer:

$$\begin{aligned} \dot{\xi}_{1i} &= \xi_{2i} + a_1(q_{mi} - \xi_{1i}) \\ \dot{\xi}_{2i} &= \xi_{3i} + a_2(q_{mi} - \xi_{1i}) \\ \dot{\xi}_{3i} &= \xi_{4i} + a_3(q_{mi} - \xi_{1i}) \\ \dot{\xi}_{4i} &= a_4(q_{mi} - \xi_{1i}), \quad i = 1, 2, 3 \end{aligned} \tag{13}$$

where $\xi_{1i} = \hat{q}_{mi}, \xi_{2i} = \hat{\dot{q}}_{mi}, \xi_{3i} = \hat{\ddot{q}}_{mi}, \xi_{4i} = \hat{\dddot{q}}_{mi}$ represent the estimated desired position, velocity, acceleration, and jerk. a_1, a_2, a_3, a_4 are design parameters which can be specified by pole placement method. The estimation errors, seen as the lumped disturbances, can be addressed by robust control.

E. LOW-LEVEL MIMO MOTION TRACKING CONTROLLER

The control objective of low level controller is to generate a control law for u so that the position tracking error $z_2 = x_2 - \hat{q}_m$ can converge to zero or be bounded. According to the last four equations of (6), a MIMO adaptive robust motion controller is proposed. Also an adaptive robust observer is developed to estimate the joint acceleration which will be used in the motion tracking controller design. The backstepping design procedure using ARC Lyapunov functions is as follows.

step 1: Figure out the desired load force P_{Ld} for P_L that achieves precise motion tracking (i.e., $x_2 \to \hat{q}_m$ if $P_L = P_{Ld}$).

Define a switching function- like quantity as

$$z_3 = \dot{z}_2 + K_2 z_2 = x_3 - \dot{q}_r, \quad \dot{q}_r \triangleq \dot{\hat{q}}_m - K_2 z_2 \tag{14}$$

where K_2 is any positive diagonal matrix. With $G_p(s) = z_2(s)/z_3(s) = diag\{\frac{1}{s+K_{2i}}, i = 1, 2, 3\}$ as a stable

transfer function matrix, the rest design is to make z_3 small. Define $Bx_3 = Y_B(x_3)B_\theta$. Differentiating (14) while noting (6) and property 3, the dynamics of z_3 is as follows

$$M_{Sp3}\dot{z}_3 + C_{Sp3}z_3 = hP_L + J^T F_{hm} - f_0 - Y\beta - Y_B B_\theta + \Delta_{3n} + \Delta_3 \quad (15)$$

The resulting ARC control law P_{Ld} is constructed as

$$\begin{aligned} P_{Ld} &= P_{Lda} + P_{Lds} \\ P_{Lda} &= h^{-1}(f_0 + Y\hat{\beta} + Y_B\hat{B}_\theta - \hat{\Delta}_{3n} - J^T F_{hm}) \\ P_{Lds} &= h^{-1}(-K_{3s1}z_3) + P_{Ldsn} \\ \phi_3 &= \begin{bmatrix} -Y & -Y_B & I_{3\times3} & 0_{3\times1} & 0_{3\times3} \end{bmatrix}^T \\ K_{3s1} &= g_3\|\Gamma_2\phi_3\|^2 + K_3 \end{aligned} \quad (16)$$

where P_{Lda} and P_{Lds} represent the model compensation and robust feedback term, respectively. K_{3s1} and Γ_2 represent the positive definite matrix for linear feedback and adaptation rate, respectively. $K_3 > 0, g_3 > 0$. P_{Ldsn} is a robust control function having the following two properties:

$$\begin{aligned} z_3^T\left(-\phi_3^T\tilde{\theta}_q + \Delta_3 + hP_{Ldsn}\right) &\le \varepsilon_3 \\ z_3^T hP_{Ldsn} &\le 0 \end{aligned} \quad (17)$$

where $\varepsilon_3 > 0$ is a design parameter. $\tilde{\theta}_q = \hat{\theta}_q - \theta_q$ is the parameter estimation error. Let $z_4 = P_L - P_{Ld}$, then the third error subsystem becomes

$$M_{Sp3}\dot{z}_3 + C_{Sp3}z_3 = hP_{Ldsn} + hz_4 - K_{3s1}z_3 - \phi_3^T\tilde{\theta}_q + \Delta_3 \quad (18)$$

step 2: Figure out the desired flow Q_{Ld} for Q_L such that the actual load force tracks the desired load force synthesized in Step 1.

As seen from (18), precise motion tracking can be achieved if $z_4 = 0$. Therefore, in this part, a control function should be generated such that z_4 converges to zero or to be bounded. In the ARC backstepping design, the feedback of joint acceleration $\ddot{q}$ is necessary when computing $\dot{P}_{Ld}$ for adaptive model compensation. Here, without measuring the joint acceleration directly, the estimates of the joint velocity and acceleration are obtained through the following adaptive robust observer [27], [28].

Observer Design

The following observer errors are defined

$$\begin{aligned} e_{o1} &= x_2 - y \\ e_{o2} &= \dot{e}_{o1} + K_{o1}e_{o1} = x_3 - \dot{y}_r, \quad \dot{y}_r \triangleq \dot{y} - K_{o1}e_{o1} \end{aligned} \quad (19)$$

where y and $\dot{y}_r$ represent the estimates of $x_2 = q$ and $x_3 = \dot{q}$ respectively. K_{o1} is any positive feedback gain matrix. The proposed nonlinear observer is :

$$\bar{M}_{Sp3}\ddot{y}_r = hP_L + J^T F_{hm} - \bar{C}_{Sp3}\dot{y}_r - \bar{G}_{Sp3} - \bar{B}\dot{y}_r + \bar{\Delta}_{3n} + T_{os} + (K_{o2} + K_{o2s})e_{o2} \quad (20)$$

where $\bar{M}_{Sp3}, \bar{C}_{Sp3}, \bar{G}_{Sp3}, \bar{B}$ and $\bar{\Delta}_{3n}$ are the estimates of related matrices in which a new set of parameter estimation named as $\bar{\theta}_q$ is used. K_{o2} is positive definite matrix for linear feedback. K_{o2s} is the nonlinear feedback gain which will be specified later. T_{os} is the robust feedback term.

Noting the third equation of (6), the derivative of e_{o2} can be calculated as

$$\begin{aligned} M_{Sp3}\dot{e}_{o2} + C_{Sp3}e_{o2} = &(\bar{M}_{Sp3} - M_{Sp3})\ddot{y}_r + (\bar{C}_{Sp3} \\ &- C_{Sp3})\dot{y}_r + (\bar{G}_{Sp3} - G_{Sp3}) \\ &- Be_{o2} + (\bar{B} - B)\dot{y}_r + \Delta_{3n} \\ &- \bar{\Delta}_{3n} + \Delta_3 - T_{os} \\ &- (K_{o2} + K_{o2s})e_{o2} \end{aligned} \quad (21)$$

where

$$\begin{aligned} \ddot{y}_r = \bar{M}_{Sp3}^{-1}(&hP_L + J^T F_{hm} - \bar{C}_{Sp3}\dot{y}_r - \bar{G}_{Sp3} \\ &- \bar{B}\dot{y}_r + \bar{\Delta}_{3n} + T_{os} + (K_{o2} + K_{o2s})e_{o2}) \end{aligned} \quad (22)$$

Define

$$\begin{aligned} \ddot{y}_{r1} = &\bar{M}_{Sp3}^{-1}(hP_L + J^T F_{hm} - \bar{C}_{Sp3}\dot{y}_r - \bar{G}_{Sp3} \\ &- \bar{B}\dot{y}_r + \bar{\Delta}_{3n} + (K_{o2} + K_{o2s})e_{o2}) \\ \phi_o^T\tilde{\theta}_{qo} = &(\bar{M}_{Sp3} - M_{Sp3})\ddot{y}_{r1} + (\bar{C}_{Sp3} - C_{Sp3})\dot{y}_r \\ &+ (\bar{G}_{Sp3} - G_{Sp3}) + (\bar{B} - B)\dot{y}_r + \Delta_{3n} - \bar{\Delta}_{3n} \end{aligned} \quad (23)$$

where $\tilde{\theta}_{qo} = \bar{\theta}_q - \theta_q$. Thus (21) becomes

$$\begin{aligned} M_{Sp3}\dot{e}_{o2} + C_{Sp3}e_{o2} = &-(K_{o2} + K_{o2s})e_{o2} - Be_{o2} \\ &- (I - (\bar{M}_{Sp3} - M_{Sp3})\bar{M}_{Sp3}^{-1})T_{os} \\ &+ \phi_o^T\tilde{\theta}_{qo} + \Delta_3 \end{aligned} \quad (24)$$

If the parameter estimation error $\tilde{\theta}_{qo}$ makes $\|(\bar{M}_{Sp3} - M_{Sp3})\bar{M}_{Sp3}^{-1}\| < 1$, then there exist a robust control function $T_{os}(q, \dot{q}, \bar{\theta}, y, \dot{y})$ having the following two properties:

$$\begin{aligned} e_{o2}^T[-(I - (\bar{M}_{Sp3} - M_{Sp3})\bar{M}_{Sp3}^{-1})T_{os} + \phi_o^T\tilde{\theta}_{qo} + \Delta_3] &\le \varepsilon_o \\ - e_{o2}^T(I - (\bar{M}_{Sp3} - M_{Sp3})\bar{M}_{Sp3}^{-1})T_{os} &\le 0 \end{aligned} \quad (25)$$

where ε_o is a design parameter. $\bar{\theta}_q$ is updated via the adaptation law below

$$\dot{\bar{\theta}}_q = -Proj(\Gamma_o\phi_o^T e_{o2}) \quad (26)$$

Replacing the joint velocity $\dot{q}$ with its estimate $\dot{y}_r$ in the control law P_{Ld}, the estimate of P_{Ld} named as $\hat{P}_{Ld} = P_{Ld}(q, \dot{y}_r, \hat{\theta}_q, t)$ can be obtained. Let $\hat{z}_4 = P_L - \hat{P}_{Ld}$ be the new load force tracking error. Then (18) becomes

$$M_{Sp3}\dot{z}_3 + C_{Sp3}z_3 = hP_{Ldsn} + h\hat{z}_4 - K_{3s1}z_3 - \phi_3^T\tilde{\theta}_q + \Delta_3 + \mu \quad (27)$$

where $\mu = h(\hat{P}_{Ld} - P_{Ld})$ represents the effect of the observer error, which has the following property.

lemma 1: μ is bounded by

$$\|\mu(q, \dot{y}_r, \hat{\theta}_q, e_{o2}, z_3, t)\| \le \sigma_e(q, \dot{y}_r, \hat{\theta}_q, e_{o2}, z_3, t)\|e_{o2}\| \quad (28)$$

where σ_e is a positive scalar function.

Proof: Replacing $\dot{y}_r$ for $\dot{q}$ in z_3 and $\ddot{q}_r$, we obtain their estimates $\hat{z}_3$ and $\ddot{q}_r$ as

$$\begin{aligned}\hat{z}_3 &= \dot{y}_r - \dot{q}_r = z_3 - e_{o2}\\ \hat{\ddot{q}}_r &= \ddot{q}_r + K_1 e_{o2}, \quad \dot{y}_r = \dot{q} - e_{o2}\end{aligned} \tag{29}$$

Thus all estimation errors are at least a linear function of the observer error e_{o2} and are zero when $e_{o2} = 0$, which leads to lemma 1.

The following is to synthesis the desired flow Q_{Ld} for Q_L such that $\hat{z}_4 = P_L - \hat{P}_{Ld}$ converges to zero or be bounded. From (6), the derivative of $\hat{z}_4$ is calculated as

$$\begin{aligned}\dot{\hat{z}}_4 = Q_L\beta_e - q_v x_3\beta_e + \Delta_{4n} + \Delta_4 - \frac{\partial \hat{P}_{Ld}}{\partial x_2}x_3\\ - \frac{\partial \hat{P}_{Ld}}{\partial \dot{y}_r}\ddot{y}_r - \frac{\partial \hat{P}_{Ld}}{\partial t} - \frac{\partial \hat{P}_{Ld}}{\partial \hat{\theta}_q}\dot{\hat{\theta}}_q\end{aligned} \tag{30}$$

Treating Q_L as the control input, the resulting ARC control law is constructed as:

$$\begin{aligned}Q_{Ld} &= Q_{Lda} + Q_{Lds}\\ Q_{Lda} &= \frac{1}{\hat{\beta}_e}\left(-\phi_{4c}^T\hat{\theta}_q - hz_3 + \frac{\partial \hat{P}_{Ld}}{\partial x_2}x_3 + \frac{\partial \hat{P}_{Ld}}{\partial \dot{y}_r}\ddot{y}_r + \frac{\partial \hat{P}_{Ld}}{\partial t}\right)\\ Q_{Lds} &= \frac{1}{\beta_{e\min}}\left(-K_{4s1}\hat{z}_4\right) + Q_{Lsn}\\ K_{4s1} &= g_4\|\Gamma_2\phi_4\|^2 + d_4\|\frac{\partial P_{Ld}}{\partial \hat{\theta}_q}\|^2 + K_4\end{aligned} \tag{31}$$

where Q_{Lda} and Q_{Lds} represent the model compensation and robust feedback term, respectively. $\phi_{4c} = \left[\begin{array}{ccccc}\phi_{4c1} & \phi_{4c2} & \phi_{4c3} & \phi_{4c4} & \phi_{4c5}\end{array}\right]^T$ is the vector of regressors with $\phi_{4c1} = 0_{3\times 7}, \phi_{4c2} = 0_{3\times 3}, \phi_{4c3} = 0_{3\times 3}, \phi_{4c4} = -q_v x_3, \phi_{4c5} = I_{3\times 3}$. K_{4s1} is the positive definite linear feedback gain matrix. $K_4 > 0, g_4 > 0, d_4 > 0$. ϕ_4 will be defined later. Q_{Ldsn} is a robust control function having the following two properties:

$$\begin{aligned}\hat{z}_4^T\left(-\phi_4{}^T\tilde{\theta}_q + \Delta_4 + \beta_e Q_{Lsn}\right) \le \varepsilon_4\\ \hat{z}_4^T\beta_e Q_{Ldsn} \le 0\end{aligned} \tag{32}$$

where $\varepsilon_4 > 0$ is a design constant. $\phi_4 = [*20c\phi_{4c1}\ \phi_{4c2}\ \phi_{4c3}\ \phi_{4c4}\ \phi_{4c5}]^T$ is the vector of regressors of which all the elements are the same as ϕ_{4c} except $\phi_{44} = Q_{La} - q_v x_3$. The fourth error subsystem becomes

$$\begin{aligned}\dot{\hat{z}}_4 = -hz_3 - \frac{\beta_e}{\beta_{e\min}}\left(K_{4s1}\hat{z}_4\right)\\ + (-\phi_4{}^T\tilde{\theta}_q + \Delta_4 + \beta_e Q_{Lsn}) - \frac{\partial \hat{P}_{Ld}}{\partial \hat{\theta}_q}\dot{\hat{\theta}}_q\end{aligned} \tag{33}$$

Like $\hat{\theta}_F$, the adaptation law for $\hat{\theta}_q$ is designed as:

$$\dot{\hat{\theta}}_q = Proj(\Gamma_2(\phi_3 z_3 + \phi_4\hat{z}_4)) \tag{34}$$

where $\Gamma_2 > 0$ is a positive definite adaptation rate matrix.

Finally, the control voltage of the valves can be obtained by:

$$u_i = \frac{Q_{Ldi}}{k_{q1i}\frac{A_{1i}}{V_{1i}}\sqrt{|\Delta P_{1i}|} + k_{q2i}\frac{A_{2i}}{V_{2i}}\sqrt{|\Delta P_{2i}|}}, i = \{1, 2, 3\} \tag{35}$$

F. MAIN RESULTS

Following the standard ARC arguments shown in[19], [29], and [30], the following theoretical results can be obtained.

Theorem 1: In the inner loop (low level motion tracking), if the control gain matrices are chosen such that $\lambda_{\min}(K_{o2}) \ge k_{o2}, \lambda_{\min}(K_{o2s}) \ge 1/2\sigma_e^2, \lambda_{\min}(K_3) \ge k_3 + 1/2, \lambda_{\min}(K_4) \ge k_4, g_3 > \frac{2}{4d_4}, g_4 > \frac{2}{4d_4}$, the control law (35) can guarantee the bounded motion tracking errors and observer errors by

$$V_{s4}(t) \le \exp(-\lambda t)V_{s4}(0) + \frac{\varepsilon}{\lambda}[1 - \exp(-\lambda t)] \tag{36}$$

where

$$\begin{aligned}V_{s4} &= \frac{1}{2}(e_{o2}^T M_{Sp3}e_{o2} + z_3^T M_{Sp3}z_3 + \hat{z}_4^T\hat{z}_4),\\ \lambda &= 2\min\{\frac{\lambda_{\min}(K_3)}{\sup_t\{\lambda_{\max}(M_{Sp3}(t))\}}, \frac{\beta_e}{\beta_{e\min}}\lambda_{\min}(K_4),\\ &\quad \frac{\lambda_{\min}(K_{o2})}{\sup_t\{\lambda_{\max}(M_{Sp3}(t))\}}\}, \varepsilon = \varepsilon_o + \varepsilon_3 + \varepsilon_4.\end{aligned}$$

Furthermore, if, after a finite time, $\Delta_i = 0, i = 3, 4$, zero final tracking error can be achieved, i.e., $z_2 \to 0$, as $t \to \infty$.

Proof of Theorem 1: Differentiate V_{s4} while noting (24), (27) and (33) and property 2, one can obtain

$$\begin{aligned}\dot{V}_{s4} &= e_{o2}^T(M_{Sp3}\dot{e}_{o2} + \frac{1}{2}\dot{M}_{Sp3}e_{o2}) + z_3^T(M_{Sp3}\dot{z}_3\\ &\quad + \frac{1}{2}\dot{M}_{Sp3}z_3) + \hat{z}_4^T\dot{\hat{z}}_4\\ &= e_{o2}^T(M_{Sp3}\dot{e}_{o2} + C_{Sp3}e_{o2}) + z_3^T(M_{Sp3}\dot{z}_3\\ &\quad + C_{Sp3}z_3) + \hat{z}_4^T\dot{\hat{z}}_4\\ &= -e_{o2}^T(K_{o2} + K_{o2s})e_{o2} - e_{o2}^T B e_{o2}\\ &\quad - e_{o2}^T[(I - (\bar{M}_{Sp3} - M_{Sp3})\bar{M}_{Sp3}^{-1})T_{os}\\ &\quad + \phi_o^T\tilde{\theta}_{qo} + \Delta_3] + z_3^T(hP_{Ldsn} - \phi_3^T\tilde{\theta}_q + \Delta_3)\\ &\quad - z_3^T K_{3s1}z_3 + z_3^T\mu - \hat{z}_4^T\frac{\beta_e}{\beta_{e\min}}\left(K_{4s1}\hat{z}_4\right)\\ &\quad + \hat{z}_4^T(-\phi_4{}^T\tilde{\theta}_q + \Delta_4 + \beta_e Q_{Lsn}) - \hat{z}_4^T\frac{\partial \hat{P}_{Ld}}{\partial \hat{\theta}_q}\dot{\hat{\theta}}_q\end{aligned} \tag{37}$$

With the adaptation law of (34), noting the characteristics of the projection mapping

$$\begin{aligned}\|\dot{\hat{\theta}}_q\|^2 &= \|Proj(\Gamma_2(\phi_3 z_3 + \phi_4\hat{z}_4))\|^2\\ &\le \|\Gamma_2(\phi_3 z_3 + \phi_4\hat{z}_4)\|^2\\ &\le 2(\|\Gamma_2\phi_3\|^2 z_3^2 + \|\Gamma_2\phi_4\|^2\hat{z}_4^2)\end{aligned} \tag{38}$$

Thus, if $g_3 > \frac{2}{4d_4}$, $g_4 > \frac{2}{4d_4}$, then

$$\begin{aligned}|\hat{z}_4^T \frac{\partial \hat{P}_{Ld}}{\partial \hat{\theta}_q}\dot{\hat{\theta}}_q| &\le (d_4\|\frac{\partial \hat{P}_{Ld}}{\partial \hat{\theta}_q}\|^2\|\hat{z}_4\|^2 + \frac{1}{4d_4}\|\dot{\hat{\theta}}_q\|^2)\\ &\le d_4\|\frac{\partial \hat{P}_{Ld}}{\partial \hat{\theta}_q}\|^2\|\hat{z}_4\|^2 + g_3\|\Gamma_2\phi_3\|^2\|z_3\|^2\\ &\quad + g_4\|\Gamma_2\phi_4\|^2\|\hat{z}_4\|^2 \end{aligned} \tag{39}$$

Noting (17), (25), (32), (37) becomes

$$\begin{aligned}\dot{V}_{s4} \le& -e_{o2}^T(K_{o2}+K_{o2s})e_{o2} - e_{o2}^T B e_{o2} - z_3^T K_3 z_3\\ &+ z_3^T\mu - \hat{z}_4^T\frac{\beta_e}{\beta_{e\min}}\left(K_4\hat{z}_4\right) + \varepsilon_o + \varepsilon_3 + \varepsilon_4 \end{aligned} \tag{40}$$

If the gain matrices satisfy the conditions in Theorem 1, by completion of square, we have

$$\begin{aligned}\dot{V}_{s4} &\le -[k_{o2} + \lambda_{min}(K_{o2s})]\|e_{o2}\|^2 - (k_3 + 1/2)\|z_3\|^2\\ &\quad + \|z_3\|\sigma_e\|e_{o2}\| - \frac{\beta_e}{\beta_{e\min}}k_4\|z_4\|^2 + \varepsilon_o + \varepsilon_3 + \varepsilon_4\\ &\le -k_{o2}\|e_{o2}\|^2 - k_3\|z_3\|^2 - \frac{\beta_e}{\beta_{e\min}}k_4\|z_4\|^2\\ &\quad + \varepsilon_o + \varepsilon_3 + \varepsilon_4\\ &\le -\lambda V_{s4} + \varepsilon \end{aligned} \tag{41}$$

which lead to (36).

When $\Delta_3 = 0$, $\Delta_4 = 0$, choose a function $V_{a4} = V_{s4} + \frac{1}{2}\tilde{\theta}_q^T\Gamma_2^{-1}\tilde{\theta}_q + \frac{1}{2}\tilde{\theta}_{qo}^T\Gamma_o^{-1}\tilde{\theta}_{qo}$. Differentiate V_{a4} while noting the adaptation law (26) and (34), one can obtain

$$\begin{aligned}\dot{V}_{a4} &= \dot{V}_{s4} + \tilde{\theta}_q^T\Gamma_2^{-1}\dot{\tilde{\theta}}_q + \tilde{\theta}_{qo}^T\Gamma_o^{-1}\dot{\tilde{\theta}}_{qo}\\ &\le -e_{o2}^T(K_{o2}+K_{o2s})e_{o2} - z_3^T K_{3s1} z_3 + z_3^T\mu\\ &\quad - \hat{z}_4^T\frac{\beta_e}{\beta_{e\min}}\left(K_{4s1}\hat{z}_4\right) - \hat{z}_4^T\frac{\partial \hat{P}_{Ld}}{\partial \hat{\theta}_q}\dot{\hat{\theta}}_q\\ &\quad + \tilde{\theta}_q^T\Gamma_2^{-1}(Proj(\Gamma_2(\phi_3 z_3 + \phi_4 z_4))\\ &\quad - \Gamma_2(\phi_3 z_3 + \phi_4 z_4)) + \tilde{\theta}_{qo}^T\Gamma_o^{-1}(Proj(\Gamma_o(-\phi_o e_{o2}))\\ &\quad - \Gamma_o(-\phi_o e_{o2}))\\ &\le -e_{o2}^T(K_{o2}+K_{o2s})e_{o2} - z_3^T K_{3s1} z_3 + z_3^T\mu\\ &\quad - \hat{z}_4^T\frac{\beta_e}{\beta_{e\min}}\left(K_{4s1}\hat{z}_4\right) - \hat{z}_4^T\frac{\partial \hat{P}_{Ld}}{\partial \hat{\theta}_q}\dot{\hat{\theta}}_q\\ &\le -k_{o2}\|e_{o2}\|^2 - k_3\|z_3\|^2 - \frac{\beta_e}{\beta_{e\min}}k_4\|z_4\|^2 \end{aligned} \tag{42}$$

Therefore, e_{o2}, z_3, $z_4 \in L_2$. Also $\dot{z}$ can be proved to be bounded. So, $z \to 0$ as $t \to \infty$ by the barbalat's lemma. Since the transfer function matrices $G_p(s) = z_2(s)/z_3(s) = diag\{1/(s + K_{2i}), i = 1, 2, 3\}$ and $G_o(s) = e_{o1}(s)/e_{o2}(s) = diag\{1/(s + K_{o1i}), i = 1, 2, 3\}$ are stable transfer functions, z_2 and e_{o1} will also converge to zero exponentially.

Theorem 2: In the outer loop (high level human motion intent inference), if the zero tracking error $z_{2h} = 0$ is achieved in the inner loop, the control law (9) can guarantee the bounded tracking error of the human-machine interaction force by

$$V_{s1}(t) \le \exp(-\lambda_1 t)V_{s1}(0) + \frac{\varepsilon_1}{\lambda_1}[1 - \exp(-\lambda_1 t)] \tag{43}$$

where $V_{s1} = (1/2)z_1^T K_f z_1$, $\lambda_1 = 2\frac{\lambda_{\min}(k_1)}{\sup_t\{\lambda_{\max}(K_f(t))\}}$. Furthermore, if, after a finite time, $\Delta_1 = 0$ and $\dot{K}_f = 0$, force tracking error is bounded with integral asymptotically converging to zero, i.e., $z_1 \to 0$, as $t \to \infty$.

Proof of Theorem 2: Differentiate V_{s1} while noting (11), one can obtain

$$\begin{aligned}\dot{V}_{s1} &= z_1^T(K_f\dot{z}_1 + \frac{1}{2}\dot{K}_f z_1)\\ &= z_1^T(-k_1 z_1 - z_{2h} + \Delta_1 + Y_{\theta_F}\tilde{\theta}_F - x_{msn} + \frac{1}{2}\dot{K}_f z_1) \end{aligned} \tag{44}$$

If $z_{2h} = 0$, noting (10), (44) becomes

$$\begin{aligned}\dot{V}_{s1} &= -z_1^T k_1 z_1 + z_1^T\left(\Delta_1 + \frac{1}{2}\dot{K}_f z_1 + Y_{\theta_F}\tilde{\theta}_F - x_{msn}\right)\\ &\le -z_1^T k_1 z_1 + \varepsilon_1 \end{aligned} \tag{45}$$

which leads to (43).

When $\Delta_1 = 0$ and $\dot{K}_f = 0$, choose a function $V_{a1} = V_{s1} + \frac{1}{2}\tilde{\theta}_F^T\Gamma_1^{-1}\tilde{\theta}_F$. Differentiate V_{a1}, one can obtain

$$\begin{aligned}\dot{V}_{a1} &= \dot{V}_{s1} + \tilde{\theta}_F^T\Gamma_1^{-1}\dot{\tilde{\theta}}_F\\ &= -z_1^T k_1 z_1 - z_1^T x_{msn}\\ &\quad + \tilde{\theta}_F^T\Gamma^{-1}(Proj(-\Gamma_1 Y_{\theta_F} z_1) - (-\Gamma_1 Y_{\theta_F} z_1))\\ &\le -z_1^T k_1 z_1 \end{aligned} \tag{46}$$

Therefore, $z_1 \in L_2$. Also $\dot{z}_1$ can be proved to be bounded. So, $z_1 \to 0$ as $t \to \infty$ by the barbalat's lemma.

Remark 1: The proposed control algorithm is a typical cascade architecture as shown in Fig. 2. The closed-loop stability and the precise interaction force tracking can be realized if $z_{2h} = 0$ is achieved in Theorem 1. However, z_{2h} can not be 0 for all the time due to the effect of disturbance and modeling uncertainties. Thus, the traditional cascade design in which the inner loop bandwidth should be much larger than that of the outer loop (usually $5 \sim 10$ times) is necessary.

IV. SIMULATION RESULTS

A. SIMULATION SETUP

A simulation model based on (1) is set up by using Matlab/Simulink. The simulation parameters are selected part from our exoskeleton platform and part from the human data in [31]. Parameters of the 3-DOF support leg exoskeleton are: $m_s = 3.25kg$, $m_t = 7kg$, $m_{ub} = 47.5kg$, $L_s = 0.4987m$, $L_t = 0.4287m$, $L_{Gs} = 0.2828m$, $L_{Gt} = 0.2431m$, $L_{Gub} = 0.1885m$, $h_{Gub} = -0.05m$, $I_s = 0.0738kg \cdot m^2$, $I_t = 0.1342kg \cdot m^2$, $I_{ub} = 2.9676kg \cdot m^2$. Hydraulic cylinder parameters are: $A_1 = diag\{3.1416e^{-4}, 3.1416e^{-4}, 6.1575e^{-4}\}m^2$, $A_2 = diag\{1.1310e^{-4}, 1.1310e^{-4}, 4.6181e^{-4}\}m^2$, $V_{h1} = diag\{9.8960e^{-5}, 9.8960e^{-5}, 1.9396e^{-4}\}m^3$, and $V_{h2} = diag\{2.0595e{-}5, 2.0595e{-}5, 8.4096e^{-5}\}m^3$. The valve parameters are $k_{q1} = diag\{1e^{-8}, 1e^{-8}, 1e^{-8}\}\frac{m^3}{sec\sqrt{PaV}}$ and $k_{q2} = diag\{1e^{-8}, 1e^{-8}, 1e^{-8}\}\frac{m^3}{sec\sqrt{PaV}}$. The supplied pressure is $P_s = 5e^7 Pa$ and actual bulk modulus is $\beta_e = 8.7e^7 Pa$. The initial system parameter estimates are set as the real

values and the lumped disturbances are set as zero. The sampling time $t_s = 0.001s$.

B. SIMULATION RESULTS

In the following simulations, the desired human-machine interaction force is selected as zero and three low-level control algorithms are compared:

C1: Independent joint based PID control with velocity feedforward given by

$$u = -K_p z_2 - K_I \int_0^t z_2 dt - K_d \dot{z}_2 + VF\dot{x}_{2d}, \qquad (47)$$

The control gains are selected as $K_p = diag\{4, 4, 4\}$, $K_I = diag\{50, 50, 50\}$, $K_d = diag\{6, 6, 6\}$, $VF = diag\{0.1, 0.1, 0.1\}$.

C2: The controller proposed in section $III - E$ but with the adaptation turned off. The control gains are selected as $K_2 = diag\{30, 30, 30\}$, $K_3 = diag\{200, 100, 100\}$, $K_4 = diag\{200, 100, 100\}$, $K_{o1} = diag\{60, 60, 60\}$, $K_{o2} = diag\{400, 200, 200\}$, $\Gamma_o = \Gamma_2 = 0_{17\times 17}$.

C3: The controller proposed in section $III - E$. The control gains are selected as $K_2 = diag\{30, 30, 30\}$, $K_3 = diag\{200, 100, 100\}$, $K_4 = diag\{200, 100, 100\}$, $K_{o1} = diag\{60, 60, 60\}$, $K_{o2} = diag\{400, 200, 200\}$. The adaptive rates for the first and fifth element of $\bar{\theta}_q$ and $\hat{\theta}_q$ are selected as $\gamma_{o1} = 10$, $\gamma_{o5} = 2$, $\gamma_{21} = 10$, $\gamma_{25} = 10$.

Two high-level force controllers are tested for comparison:

FDRC: The controller proposed in section $III - C$ but with the adaptation turned off.

FARC: The controller proposed in section $III - C$.

To verify the effectiveness of these controllers, the following test sets are performed:

Set1: To test the tracking performance of motion controllers in the low level.

Set2: Fixing the low level controller to test the force control performance using different high level algorithms.

Set3: Fixing the high level algorithm as FARC to test the force control performance using different low level algorithms.

Set4: To test the performance robustness of the proposed force controllers to load change.

In *Set1*, the adaptation law is switched off so that the influence of different control structures on motion tracking performance can be seen. Thus only C1 and C2 are compared. The sinusoid curves $x_{2d} = [-2 + 0.2\sin(\frac{\pi}{2}t - \frac{\pi}{2}),\ 0.5 + 0.2\sin(\frac{\pi}{2}t - \frac{\pi}{2}),\ 0.2\sin(\frac{\pi}{2}t - \frac{\pi}{2})]rad$ is used as the desired motion trajectory. Fig.3 shows the tracking errors and control input. Without using any model information and neglecting the coupling effect of multiple axes, the control gains of C1 are quite limited leading to large tracking errors. For C2, the control gains can be increased due to the consideration of multi-joint hydraulic exoskeleton dynamics and thus better tracking performance can be achieved.

For *Set2* and *Set3*, by passing x_{2d} in Set1 into the kinematics equations, the human motion trajectory x_h can be obtained. Table 1 shows the gains and adaptation rate

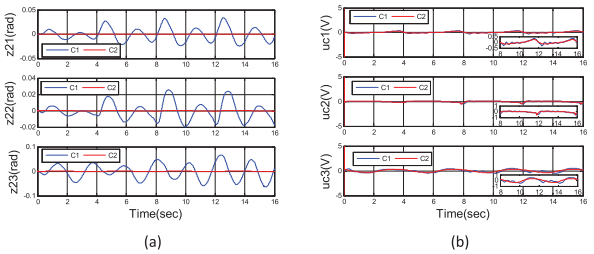

FIGURE 3. Simulation results for Set1: (a) tracking error of C1 and C2, (b) control input of C1 and C2.

TABLE 1. Controller gains of high level controllers in simulation.

	C1	C2
FARC	$k_1 = diag\{2, 2, 2\}$ $\Gamma_1 = diag\{0, 0, 0, \frac{1}{2}, \frac{1}{2}, \frac{1}{2}\}$	$k_1 = diag\{8, 8, 8\}$ $\Gamma_1 = diag\{0, 0, 0, 2, 15, 2\}$

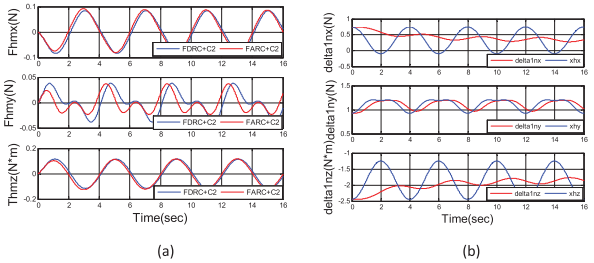

FIGURE 4. Simulation results for Set2: (a) human machine interaction force, (b) parameter estimation.

matrices of high level controllers which vary with different low level controllers. Without compromising much control performance, only Δ_{1n} is adapted in the simulation. As shown in Fig.4, due to the online parameter estimate in the high level controller(FARC), the human motion can be learned effectively, resulting in a smaller human machine interaction force over FDRC. Furthermore, Fig.5 shows that with FARC as the high level controller, cascade force controller with C2 achieves more accurate parameter estimation and more precise force control performance than that with C1. The reason is that C2 achieves higher inner loop bandwidth with all the system dynamics considered which leads to larger control gains and adaptation rate in its high level controller.

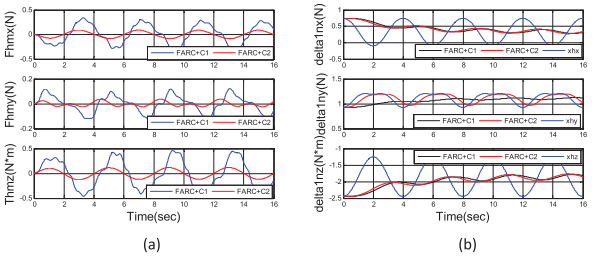

FIGURE 5. Simulation results for Set3: (a) human machine interaction force, (b) parameter estimation.

In *Set4*, a $2.72kg$ load is mounted in the shank making the parameter uncertainties exist in the first and fifth element

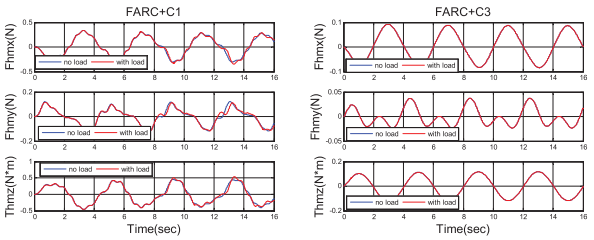

FIGURE 6. The human machine interaction force for Set4 : (a) FARC+C1, (b) FARC+C3.

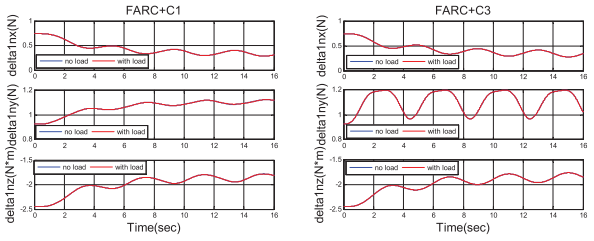

FIGURE 7. Estimation of Δ_{1n} for Set4: (a) FARC+C1, (b) FARC+C3.

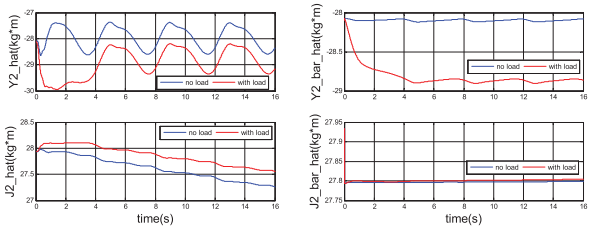

FIGURE 8. Estimations of Y_2 and J_2 of FARC+C3 for Set4: (a) estimations in the low level controller, (b) estimations in the low level observer.

of θ_q (denote as Y_2 and J_2). From Fig.6, it is seen that the proposed ARC cascade force controller(FARC+C3) achieves a more consistent performance to load variation, compared to the PID cascade controller(FARC+C1). The reason is that fast parameter adaptation in FARC+C3 as shown in Fig.7-Fig.8 makes the model uncertainties resulting from the load change be learned more quickly and then be effectively compensated.

V. CONCLUSION

In this paper, a robust control scheme is developed for the human machine interaction force control of a 3-DOF hydraulic leg exoskeleton used to augment the human performance. A cascade control structure with high level controller inferring the human motion intent and low level controller performing motion tracking is proposed. An observer is synthesized to estimate the joint acceleration which is used in the design of the low level backstepping controller. MIMO ARC algorithm is applied in the two control levels to handle the effects of various model uncertainties. Both high accuracy interaction force control and good robust performance in the presence of load change and disturbances are achieved by the proposed method, which is validated by comparative simulations.

REFERENCES

[1] J.-L. C. Racine, "Control of a lower extremity exoskeleton for human performance amplification," Ph.D. dissertation, Dept. Mech. Eng., Univ. California, Berkeley, CA, USA, 2003.
[2] H. Kazerooni, J.-L. Racine, L. Huang, and R. Steger, "On the control of the berkeley lower extremity exoskeleton (BLEEX)," in *Proc. IEEE Int. Conf. Robot. Autom.*, Apr. 2005, pp. 4353–4360.
[3] K. Kong and M. Tomizuka, "Control of exoskeletons inspired by fictitious gain in human model," *IEEE/ASME Trans. Mechatronics*, vol. 14, no. 6, pp. 689–698, Dec. 2009.
[4] W. Yu, J. Rosen, and X. Li, "PID admittance control for an upper limb exoskeleton," in *Proc. Amer. Control Conf.*, vol. 3. 2011, pp. 1124–1129.
[5] H. Lee, B. Lee, W. Kim, M. Gil, J. Han, and C. Han, "Human-robot cooperative control based on pHRI (Physical Human-Robot Interaction) of exoskeleton robot for a human upper extremity," *Int. J. Precis. Eng. Manuf.*, vol. 13, no. 6, pp. 985–992, Jun. 2012.
[6] H.-D. Lee, B.-K. Lee, W.-S. Kim, J.-S. Han, K.-S. Shin, and C.-S. Han, "Human–robot cooperation control based on a dynamic model of an upper limb exoskeleton for human power amplification," *Mechatronics*, vol. 24, no. 2, pp. 168–176, Mar. 2014.
[7] U. Nagarajan, G. Aguirre-Ollinger, and A. Goswami, "Integral admittance shaping for exoskeleton control," in *Proc. IEEE Int. Conf. Robot. Autom.*, May 2015, pp. 5641–5648.
[8] Z. Li, C. Su, L. Wang, Z. Chen, and T. Chai, "Nonlinear disturbance observer-based control design for a robotic exoskeleton incorporating fuzzy approximation," *IEEE Trans. Ind. Electron.*, vol. 62, no. 9, pp. 5763–5775, Sep. 2015.
[9] W. Huo, S. Mohammed, and Y. Amirat, "Observer-based active impedance control of a knee-joint assistive orthosis," in *Proc. IEEE Int. Conf. Rehabil. Robot.*, Aug. 2015, pp. 313–318.
[10] S. Chen *et al.*, "Adaptive robust cascade force control of 1-DOF hydraulic exoskeleton for human performance augmentation," *IEEE/ASME Trans. Mechatronics*, vol. 22, no. 2, pp. 589–600, Apr. 2017.
[11] S. Chen *et al.*, "Cascade force control of lower limb hydraulic exoskeleton for human performance augmentation," in *Proc. 42nd Annu. Conf. IEEE Ind. Electron. Soc.*, Oct. 2016, pp. 512–517.
[12] R. Volpe and P. Khosla, "An experimental evaluation and comparison of explicit force control strategies for robotic manipulators," in *Proc. IEEE Int. Conf. Robot. Autom.*, May 1992, pp. 1387–1393.
[13] E. Paljug, T. Sugar, V. Kumar, and X. Yun, "Some important considerations in force control implementation," in *Proc. IEEE Int. Conf. Robot. Autom.*, May 1992, pp. 1270–1275.
[14] B. Yao and M. Tomizuka, "Adaptive control of robot manipulators in constrained motion," in *Proc. Amer. Control Conf.*, 1993, pp. 1128–1132.
[15] J. Yao, W. Deng, and Z. Jiao, "Adaptive control of hydraulic actuators with LuGre model-based friction compensation," *IEEE Trans. Ind. Electron.*, vol. 62, no. 10, pp. 6469–6477, Oct. 2015.
[16] J. Yao, Z. Jiao, and D. Ma, "A practical nonlinear adaptive control of hydraulic servomechanisms with periodic-like disturbances," *IEEE/ASME Trans. Mechatronics*, vol. 20, no. 6, pp. 2752–2760, Dec. 2015.
[17] W. Sun, P. Huihui, and H. Gao, "Filter-based adaptive vibration control for active vehicle suspensions with electrohydraulic actuators," *IEEE Trans. Veh. Technol.*, vol. 65, no. 6, pp. 4619–4626, Jun. 2016.
[18] W. Sun, Y. Zhang, Y. Huang, H. Gao, and O. Kaynak, "Transient-performance-guaranteed robust adaptive control and its application to precision motion control systems," *IEEE Trans. Ind. Electron.*, vol. 63, no. 10, pp. 6510–6518, Mar. 2016.
[19] B. Yao and M. Tomizuka, "Adaptive robust control of SISO nonlinear systems in a semi-strict feedback form," *Automatica*, vol. 33, no. 5, pp. 893–900, May 1997.
[20] B. Yao and M. Tomizuka, "Adaptive robust control of MIMO nonlinear systems in semi-strict feedback forms," *Automatica*, vol. 37, no. 9, pp. 1305–1321, Sep. 2001.
[21] Z. Chen, B. Yao, and Q. Wang, "Accurate motion control of linear motors with adaptive robust compensation of nonlinear electromagnetic field effect," *IEEE/ASME Trans. Mechatronics*, vol. 18, no. 3, pp. 1122–1129, Jun. 2013.

[22] Z. Chen, B. Yao, and Q. Wang, "μ-synthesis-based adaptive robust control of linear motor driven stages with high-frequency dynamics: A case study," *IEEE/ASME Trans. Mechatronics*, vol. 20, no. 3, pp. 1482–1490, Jun. 2015.
[23] Z. Chen, Y.-J. Pan, and J. Gu, "Integrated adaptive robust control for multilateral teleoperation systems under arbitrary time delays," *Int. J. Robust Nonlinear Control*, vol. 26, no. 12, pp. 2708–2728, Aug. 2016.
[24] C. Hu, Z. Hu, Y. Zhu, and Z. Wang, "Advanced GTCF-LARC contouring motion controller design for an industrial X–Y linear motor stage with experimental investigation," *IEEE Trans. Ind. Electron.*, vol. 64, no. 4, pp. 3308–3318, Apr. 2017.
[25] C. Hu, Z. Wang, Y. Zhu, M. Zhang, and H. Liu, "Performance-oriented precision LARC tracking motion control of a magnetically levitated planar motor with comparative experiments," *IEEE Trans. Ind. Electron.*, vol. 63, no. 9, pp. 5763–5773, Sep. 2016.
[26] M. Yuan, Z. Chen, B. Yao, and X. Zhu, "Time optimal contouring control of industrial biaxial gantry: A highly efficient analytical solution of trajectory planning," *IEEE/ASME Trans. Mechatronics*, vol. 22, no. 1, pp. 247–257, Feb. 2017.
[27] F. Bu, "Nonlinear model based coordinated adaptive robust control of electro-hydraulic systems," Ph.D. dissertation, Dept. Mech. Eng., Purdue Univ., West Lafayette, IN, USA, 2001.
[28] F. Bu and B. Yao, "Observer based coordinated adaptive robust control of robot manipulators driven by single-rod hydraulic actuators," in *Proc. IEEE Int. Conf. Robot. Autom.*, Apr. 2000, pp. 3034–3039.
[29] B. Yao, "High performance adaptive robust control of nonlinear systems: A general framework and new schemes," in *Proc. IEEE Conf. Decision Control*, vol. 3. Dec. 1997, pp. 2489–2494.
[30] B. Yao, F. Bu, J. Reedy, and G. T. C. Chiu, "Adaptive robust motion control of single-rod hydraulic actuators: Theory and experiments," *IEEE/ASME Trans. Mechatronics*, vol. 5, no. 1, pp. 79–91, Mar. 2000.
[31] D. A. Winter, *Biomechanics and Motor Control of Human Movement*. Hoboken, NJ, USA: Wiley, 2009.

SHAN CHEN received the B.Eng. and Ph.D. degrees in mechatronic control engineering from Zhejiang University, Zhejiang, China, in 2011 and 2017, respectively. She is currently an Assistant Professor with the School of Mechanical Engineering, Hefei University of Technology, Hefei, China. Her research interests include control theory, advanced motion control of mechatronic systems, and robotics.

ZHENG CHEN (S'11–M'13) received the B.Eng. and Ph.D. degrees in mechatronic control engineering from Zhejiang University, Zhejiang, China, in 2007 and 2012, respectively. From 2013 to 2015, he was a Post-Doctoral Researcher with the Department of Mechanical Engineering, Dalhousie University, Halifax, NS, Canada. Since 2015, he has been an Associated Professor with the Ocean College, Zhejiang University. His research interests include control theory, advanced motion control of mechatronic systems, and robotics.

BIN YAO (S'92–M'96–SM'09) received the B.Eng. degree in applied mechanics from the Beijing University of Aeronautics and Astronautics, China, in 1987, the M.Eng. degree in electrical engineering from Nanyang Technological University, Singapore, in 1992 and the Ph.D. degree in mechanical engineering from the University of California at Berkeley in 1996. He has been with the School of Mechanical Engineering, Purdue University, since 1996, and was promoted to the rank of Professor in 2007. He was honored as a Kuang-Piu Professor in 2005 and a Changjiang Chair Professor at Zhejiang University, Ministry of Education, China, in 2010.